Coherent x-ray generation from below-threshold harmonics

Ji-Cai Liu,[1,2] Markus C. Kohler,[1] Christoph H. Keitel,[1] and Karen Z. Hatsagortsyan[1,*]
[1]*Max-Planck-Institut für Kernphysik, Saupfercheckweg 1, D-69117 Heidelberg, Germany*
[2]*Mathematics and Physics Department, North China Electric Power University, 102206 Beijing, People's Republic of China*
(Received 13 September 2011; published 6 December 2011)

The possibility of x-ray emission employing below-threshold-harmonic generation in the nontunneling regime is considered. The interaction of a tightly bound valence electron in a highly charged ion with intense extreme-ultraviolet laser radiation is investigated in the weakly relativistic regime by numerical solution of the two-dimensional relativistically corrected Schrödinger equation. Nondipole effects and the relativistic mass correction are taken into account by expansion of the total Klein-Gordon Hamiltonian up to the second order in the ratio between the electron velocity and the speed of light. The harmonics below the ionization energy of the tightly bound system are found to be emitted with much higher probability than the standard plateau harmonics of loosely bound systems in the tunneling ionization regime for the same photon energy. This paves a path toward coherent hard x rays.

DOI: 10.1103/PhysRevA.84.063817 PACS number(s): 42.65.Ky, 42.50.Hz

I. INTRODUCTION

As a promising way to produce coherent extreme-ultraviolet (XUV) and soft-x-ray radiation and attosecond pulses, high-order-harmonic generation (HHG) has been a leading research field in nonlinear optics [1–3]. The generation of above-threshold harmonics with energies higher than the ionization potential has been widely investigated and has been well understood by means of the semiclassical three-step model [4,5] and the quantum trajectory approach [6–9] within the strong -field approximation (SFA) [10]. In the SFA, the electron dynamics in the continuum is assumed to be dominated by the strong laser field and the influence of the Coulomb potential is neglected after tunneling. This theory explains well the main characteristics of high-order-harmonic generation above the ionization threshold, such as the plateau and cutoff of the harmonic spectrum and the intensity dependence of the phase of the dipole moment, but its description of the below- and around-threshold harmonics is not accurate due to the strong influence of the atomic potential on the electron dynamics.

Usually, low-order-harmonic generation is considered to be a nonlinear process that can be fully explained within perturbation theory. The first nonperturbative analysis of the below-threshold harmonics (BTHs) within the SFA-based quantum-orbit theory (neglecting the Coulomb field effect of the atomic core) [11] has shown that the major contribution to BTHs comes from a specific trajectory which does not belong to the usual "short-long" classification scheme and corresponds to the electron moving straight back to the atomic core from the tunneling exit, providing significantly larger HHG probability than the usual trajectories. The recent new findings of experimental studies [12,13] shed more light on the physics of the strong-field BTHs. Yost *et al.* [12] studied the vacuum-ultraviolet frequency combs from BTHs in xenon gas irradiated by an intense infrared laser field. They found that both the laser-driven continuum dynamics and the presence of the Coulomb potential contribute to the generation of BTHs. Moreover, they showed that in the BTH regime multiple emission pathways also exist, as in the case of above-threshold harmonics. The experimental study of Power *et al.* [13] found that the BTH driven by a strong mid-infrared laser field shows a nonperturbative behavior and semiclassical characteristics dominated by the long electron trajectory which can still be properly interpreted with the modified three-step model. Hostetter *et al.* [14] studied theoretically the generation of BTHs in a model atom by extending the three-step semiclassical model to include the effects of the atomic potential, obtaining a good agreement with the experimental observations [12,13]. The experimental and theoretical analysis of quantum path contributions to BTHs have been carried out in [15] and conclusions are derived for the use of BTHs in molecular spectroscopy.

The investigations of [11–15] belong to the nonrelativistic regime. Nontunneling harmonics in the weakly relativistic regime have been considered by Hu *et al.* in [16,17]. They identified a so-called "surfing" mechanism of HHG during the interaction of ultraintense laser radiation with a highly charged ion [18] which enhances a limited spectral region in the HHG spectrum within the BTHs. The latter, in contrast to the usual three-step mechanism of HHG, is explained by bound dynamics of the part of the electron wave packet which is trapped in the laser-dressed atomic potential. In this way efficient HHG up to 300 eV photon energies is shown in [16]. Can the BTHs be extended to cover the hard-x-ray domain? This would lead to tabletop sources of hard x rays alternative to the large-scale x-ray free-electron lasers [19] aimed at ultrafast imaging and time-resolved study of the electron dynamics in atoms and molecules.

The state-of-the-art technique based on the usual three-step HHG mechanism allows generation of coherent x-ray photons up to the keV energy range [20] and production of short XUV pulses of less than 100 as [21]. The most favorable conversion efficiency for nonrelativistic keV harmonics is anticipated with mid-infrared driving laser fields in a medium of pressurized gas cells [22–24]. The further increase of the driving field intensity transfers the interaction regime into the relativistic domain where the drift motion of the ionized electron in the laser field propagation direction prohibits recollision and, consequently,

*k.hatsagortsyan@mpi-k.de

suppresses the three-step HHG [25]. Moreover, for high intensities a severe phase-matching problem arises because of a large free-electron background causing phase mismatch between the driving infrared laser wave and the emitted x rays. Although various methods exist for counteracting the relativistic drift [26–36] and even for solving both issues of relativistic HHG, the drift and the phase-matching [37] problem, the HHG yield achieved is small nevertheless. This is due to fundamental limitations arising from the energy scaling of the recombination probability, the smaller macroscopic solid emission angle, and the natural decrease of the emission yield per harmonic for high intensities because the recolliding wave packet is spread over a larger energy bandwidth [37].

In this paper, we investigate the possibility for coherent hard-x-ray production up to several keV photon energies employing below-threshold harmonic generation regime with highly charged ions (HCIs) and a strong XUV driving field. HCIs with a large ionization potential $I_p \sim 100$ a.u. are applied because in the BTH regime the HHG emission frequency (ω_H) is limited by the ionization potential (I_p), i.e., $\omega_H \lesssim I_p$. A high density of HCIs is necessary for sizable HHG yield, which can be realized using an underdense plasma [38]. However, in this case a large free-electron background will exist, hindering the realization of phase matching for the emitted x rays with the driving infrared laser field. To weaken the phase-matching problem, we employ a strong XUV field to drive the harmonic generation process, as at higher frequencies the plasma refractive index is closer to one. High frequencies are also necessary to avoid the fully relativistic regime because, as we will see below, the laser magnetic-field-induced drift also has consequences for BTHs. The intensity of the driving field should be rather high and is dictated by the high ionization potential of the HCIs. Let us aim for 3 keV harmonics, which requires $I_p \approx 110$ a.u. The HHG yield increases with increasing driving field intensity up to ionization saturation, i.e., the BTHs will be most efficient when the laser intensity approaches the barrier suppression field of the HCIs: $E_{\rm BS} \approx I_p^2/4Z$ [39] (atomic units are used throughout the paper unless specified otherwise), where Z is the charge of the ionic core. For a given ionization potential, the necessary intensity of the driving field will be smaller for a multielectron HCI (at higher Z). For instance, if one uses lead ions, $I_p = 112$ a.u. is achieved at Pb^{51+} when $I_{\rm BS} \approx 1.3 \times 10^{20}$ W/cm^2. Strong XUV fields with a frequency $\omega \sim 1$ a.u. are available at the FLASH facility in DESY [40]. We will consider intensities up to 10^{20} W/cm^2, approaching the barrier suppression limit. In such HCIs the remaining core electrons are strongly bound, e.g., the barrier suppression intensity is noticeably larger for Pb^{52+} than for Pb^{51+} and increases sharply by orders of magnitude on going to inner-shell electrons. BTHs are due to the dynamics of the valence electron, and we apply the single-active-electron approximation. Our investigation is based on a direct solution of the time-dependent Schrödinger equation (TDSE) in the weakly relativistic regime. The strong laser field as well as the ionic potential are fully taken into account. The relativistic corrections are taken into account by expanding the Klein-Gordon Hamiltonian in the velocity gauge up to the second order in the ratio of the electron velocity to the speed of light.

The question arises as to whether the usual three-step HHG process could not provide the same hard-x-ray frequencies at the cutoff $\omega_H = I_p + 3.17\, U_p$. Here, $U_p = E_0^2/4\omega^2$ is the ponderomotive potential, and E_0 and ω are the laser field amplitude and the frequency, respectively. In this paper, we show the advantage of our BTH scheme in efficiency with respect to two possible three-step HHG schemes. In one case, the driving field is an XUV field with less intensity than used for the BTH case, providing the desirable harmonic frequency $\omega_H \sim 3$ keV at the cutoff of the three-step tunneling HHG scheme with a smaller ionization potential of the HCI. In the second case, the three-step tunneling HHG is used with an infrared driving laser and with an even smaller HCI charge. Both three-step HHG schemes can provide harmonic energies of 3 keV at the cutoff but with a significantly lower rate than the proposed BTH regime.

The outline of our work is as follows. Section II presents our theoretical model where we introduce the Schrödinger-type equation used for the weakly relativistic regime and the potential employed to model the HCI. The computational details are given in Sec. III and the results of the numerical simulations are discussed in Sec. IV. Our findings are summarized in Sec. V.

II. THEORETICAL MODEL

We consider the response of the highly charged ions to the laser pulse in the single-active-electron approximation [41]. In a strong laser-matter interaction, when the velocity of the detached electron promoted by the laser field is comparable with or larger than the speed of the light c, namely, $\xi = E/c\omega \geqslant 1$, the fully relativistic treatment must be adopted; see, e.g., [42]. However, relativistic effects already start to play a role in atomic processes when the relativistic parameter is smaller than 1. Thus, the recollision-based effects, such as HHG and nonsequential double ionization, are influenced by the relativistic drift when the drift distance becomes comparable with the recolliding-electron wave packet size [43], which happens already at intensities above 3×10^{16} W/cm^2 in infrared fields ($\xi \gtrsim 0.14$). In the weakly relativistic regime with $\xi \lesssim 1$, which is the regime considered in this paper, the main deviations from the nonrelativistic dynamics are the breakdown of the dipole approximation and correspondingly the drift caused by the magnetic component of the laser field, and the relativistic mass shift [25]. Therefore, we expand the fully relativistic Hamiltonian up to the second-order corrections in the ratio of the electron velocity to the speed of light, and neglect the higher-order terms. Then, the Hamiltonian of an electron in a laser field interacting with a binding potential in the velocity gauge is given by

$$H(\boldsymbol{r},t) = \frac{1}{2}[\hat{\boldsymbol{p}} + \boldsymbol{A}(\boldsymbol{r},t)/c]^2 - \frac{1}{8c^2}[\hat{\boldsymbol{p}} + \boldsymbol{A}(\boldsymbol{r},t)/c]^4 + V(r), \tag{1}$$

where $\hat{\boldsymbol{p}}$ is the canonical momentum operator, $\boldsymbol{A}(\boldsymbol{r},t)$ is the vector potential of the laser field, and $V(r)$ is the Coulomb potential. The second term on the right-hand side is the relativistic mass shift. We do not adopt the dipole approximation for the vector potential and in this way include the magnetic field effects. We assume that the laser field is linearly polarized along the x direction and propagates in the z direction. In this

case, the dynamics of the electron induced by the laser field is mainly confined in the (x,z) plane, so it is accurate enough to solve the two-dimensional (2D) TDSE. We will further justify the reduction to 2D at the end of Sec. IV. In order to model the Coulomb field experienced by the active electron, the 2D "soft-core" potential

$$V(x,z) = -\frac{q}{\sqrt{x^2+z^2+a^2}} \tag{2}$$

is employed, which can reproduce the main features of the laser-atom interaction in the strong-field regime. The choice of the q and a parameters determines the depth of the potential and its smoothness at the origin [as a rule of thumb $q \sim Z$ is the charge of the ionic core and $a \sim N_e/(N_e + Z - 1)$ the radius of the HCI, where N_e is the number of electrons in the HCI].

The laser-driven photoemission from an isolated ion in the laser propagation direction can be obtained from the time-dependent electron acceleration in the polarization direction, $a_x(t) = \frac{\partial^2}{\partial t^2}\langle x\rangle$. The dipole approximation for the emitted light is applied because the harmonic wavelength at 3 keV ($\lambda_H \sim 5$ Å) is larger than the HCI size: $\lambda_H \gg a$. Harmonic emission taking retardation effects into account is treated, e.g., in [44]. By application of the Ehrenfest theorem, the expectation value of the acceleration is expressed as [45]

$$a_x(t) = \langle\psi(t)| - \frac{\partial}{\partial x}V(x,z) - E_x(z,t)|\psi(t)\rangle, \tag{3}$$

where $E_x(z,t) = -\frac{1}{c}\frac{\partial}{\partial t}A_x(z,t)$ is the laser electric field. The time-dependent electronic wave packet $\psi(t)$ is obtained by numerical integration of the 2D TDSE with the Hamiltonian of Eq. (1). The single-ion emission spectrum is proportional to the power spectrum of acceleration of the time-dependent atomic dipole,

$$\sigma(\omega) \propto |a_x(\omega)|^2 = \left|\frac{1}{T_2 - T_1}\int_{T_1}^{T_2} dt\, e^{-i\omega t} a_x(t)\right|^2. \tag{4}$$

To investigate the detailed spectral-temporal structures of the harmonic emission, we perform a time-frequency analysis of the electron acceleration via window Fourier transform:

$$a_x(t,\omega) = \int dt' a_x(t') e^{-i\omega t'} \exp[-(t-t')^2/\Delta t], \tag{5}$$

where Δt is the width of the time window.

III. COMPUTATIONAL DETAILS

We solve directly the weakly relativistic TDSE. The grid-based solution allows us to treat the laser field and the atomic potential on an equal footing, which is necessary to describe harmonics with photon energies below and close to the ionization threshold. The spectral method [46] is employed for solving the TDSE in Cartesian coordinates with a split-operator algorithm [47]. Within the dipole approximation, the total Hamiltonian can be written in two parts, namely, the kinetic energy and the potential energy operators. The momentum space is the eigenspace of the kinetic energy operator, while the potential term can act directly on the wave function in the coordinate space. Therefore, the TDSE can be efficiently solved by Fourier transform of the wave function back and forth between the momentum and the coordinate spaces with a fast-Fourier-transform algorithm; this is accurate enough to perform the time-dependent propagation with second-order splitting propagators for a sufficiently small time step. Generally speaking, the split-operator algorithm is not applicable in the nondipole approximation case because of the existence of the cross terms of the canonical momentum operator $\hat{\boldsymbol{p}}$ and the vector potential $\boldsymbol{A}(\boldsymbol{r},t)$. However, there is an exception for a linearly polarized laser field for which the vector potential polarized along the x direction is only a function of the coordinate along the propagation direction z. In this case, the split-operator method can be applied to the nondipole terms such as $p_x(t)A_x(z,t)$ and $p_x(t)^2A_x(z,t)$ by keeping the z component of the wave function in the coordinate space and Fourier transformation of the x component into the momentum space [17,18,25].

The electronic wave packet will extensively spread out in the space domain due to strong-field photoionization. In this case, the accurate numerical solution of the TDSE requires a quite dense and huge number of grid points to account for the motion of the detached electron in the continuum energy region. As one can see from Eq. (3), the dominant contribution to the acceleration comes from the region near the ion core, $a_x(t) \sim \langle\partial V/\partial x\rangle \sim x/r^3$. Therefore, the integration required to calculate this expectation value can be truncated at places where the force on the electron is negligible. The finite grid size employed for the propagation of the wave function causes the problem of unphysical reflections of the wave packet at the boundary and will give rise to spurious HHG [48]. The reflection can be minimized by introducing an absorbing component into the atomic potential or using mask functions. We use here a broad and smooth masking function of the form

$$M(x_i) = \cos^{1/8}\frac{|x_i - x_b|\pi}{2d_m}, \tag{6}$$

where d_m is the length of the absorbing region over which M changes smoothly from 1 to 0, and x_b are the boundary points along the integrated coordinate x_i.

The initial electronic wave packet is assumed to be the ground state of the potential $V(x,z)$; see Eq. (2). For a certain ionization potential, the values of the parameters q and a can be determined from the eigenvalue solution of the Schrödinger equation by the spectral method [46]. In this paper, atomic systems with ionization energies of 112.2 a.u. ($q = 52$, $a = 0.3735$ a.u.), 32.54 a.u. ($q = 21$, $a = 0.48094$ a.u.), and 4.42 a.u. ($q = 5$, $a = 0.6993$ a.u.) are used, which correspond approximately to the ground-state energies of Pb^{51+}, Kr^{20+}, and Ne^{4+}, respectively.

The vector potential of the laser field has five-cycle linear turn-on and turn-off ramps,

$$A_x(z,t) = \begin{cases} A_0 \frac{t-\frac{z}{c}}{t_{\rm on}} \cos\left[\omega\left(t-\frac{z}{c}\right)+\phi_0\right], & 0 < t-\frac{z}{c} \leqslant t_{\rm on}, \\ A_0 \cos\left[\omega\left(t-\frac{z}{c}\right)+\phi_0\right], & t_{\rm on} < t-\frac{z}{c} \leqslant t_{\rm on}+t_{\rm top}, \\ A_0 \frac{T_{\rm tot}-\left(t-\frac{z}{c}\right)}{t_{\rm off}} \cos\left[\omega\left(t-\frac{z}{c}\right)+\phi_0\right], & t_{\rm on}+t_{\rm top} < t-\frac{z}{c} \leqslant T_{\rm tot}, \end{cases} \tag{7}$$

where $\omega = 2\pi/T$ is the angular frequency and ϕ_0 is the carrier-envelope phase of the pulse, $t_{\rm top} = 10T$ is the duration of the field with a constant amplitude A_0, $t_{\rm on} = t_{\rm off} = 5T$ is the duration of the turn-on and turn-off ramps, and $T_{\rm tot} = t_{\rm on} + t_{\rm top} + t_{\rm off} = 10T$ is the whole pulse duration.

IV. RESULTS AND DISCUSSION

In this section we present the results of numerical calculations on x-ray generation up to the 3 keV photon energy region via BTH. A comparison of the BTH scheme with the possible three-step tunneling HHG schemes is carried out as well.

The BTH spectra for a tightly bound electron in the soft-core potential with $I_p = 112.2$ a.u. ≈ 3.06 keV (corresponding to the ground-state energy of the Pb^{51+} ion) are obtained by the numerical integration of the 2D weakly relativistic TDSE. The laser pulse contains 20 optical cycles with five-cycle linear turn-on and -off ramps specified in Eq. (7). The spectra shown in Fig. 1 are calculated from the Fourier transform of the dipole acceleration of Eq. (3) over the ten optical cycles during which the field amplitude of Eq. (7) is constant. The latter will exclude the contribution to the HHG because of the nonadiabatic evolution of the atomic system in the laser pulse. The laser intensity is 2×10^{20} W/cm^2 which is close to the barrier suppression intensity. Two cases are considered with the incident photon energies of 3 and 1 a.u., which correspond to a weakly relativistic regime with $\xi = 0.18$ and 0.55, respectively; see also Table I. These intensities are slightly above the typical beam parameters of FLASH in Hamburg, given by a peak power of 5 GW [40] and corresponding to an intensity of 5×10^{17}W/cm^2 when focused to a micrometer spot size. The ionization probability at the end of the pulse is 0.86 at $\omega = 3$ a.u. and 0.89 at $\omega = 1$ a.u.. The dimensions of the integration box for the numerical solutions, $L_z = 40$ a.u. and $L_x = 200$ a.u., are taken to be much larger than the electron excursion amplitudes $\alpha_0 = E_0/\omega^2$, which are 8.39 and 75.49 a.u., respectively, and the spatial and temporal grids with the respective step values of $dx = 9.76 \times 10^{-3}$ a.u., $dt = 2.56 \times 10^{-3}$ a.u. and $dx = 2.4 \times 10^{-2}$ a.u., $dt = 4.79 \times 10^{-4}$ a.u. are dense enough to get converged spectra. The harmonics $\omega_H \lesssim I_p$ are due to a nontunneling mechanism, which can be proved by calculating HHG with a smaller box size; see Fig. 2. Decrease in the size of the simulation box from $L_x = 40$ a.u. to $L_x = 10$ a.u. does not modify the HHG spectrum noticeably up to harmonic frequencies $\omega_H \sim 100$ a.u., while the emission of higher harmonic frequencies is decreased. One can deduce that the excursion of the electron wave packet out of the atomic size has no effect on BTH. Both of the spectra at $I_p = 112.2$ a.u. show an enhancement of BTH at $\omega_H \approx 20$ a.u. as in the case of $\omega = 3$ a.u. as well as at $\omega = 1$ a.u. As the enhancement position does not depend on the driving frequency but only on the atomic potential and the driving laser field intensity, we attribute it to the bound-bound transition resonance.

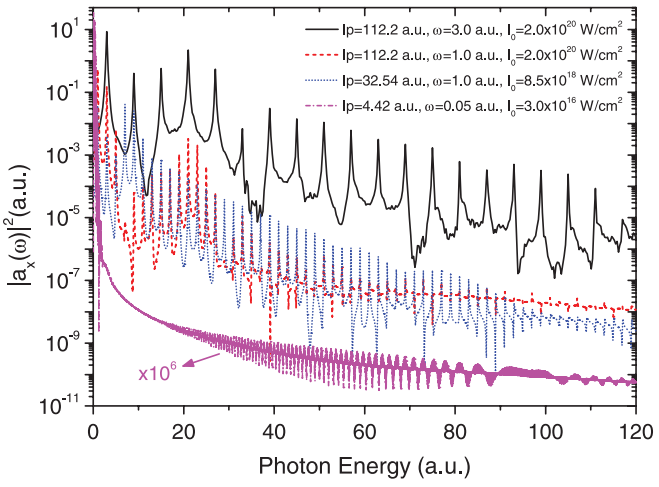

FIG. 1. (Color online) The HHG spectra for an electron in the soft-core potential of Eq. (2) with parameters shown in Table I. The spectrum for $I_p = 4.42$ a.u. (purple line, lowest curve) is multiplied by 10^6.

In the following, the efficiency of the BTH generated from the tightly bound system is investigated. We show in Fig. 1 the HHG spectra for parameters where the standard three-step mechanism is present, which provide the same hard-x-ray frequencies in the plateau (cutoff) of the spectra, using HCIs with a weaker ionization potential. For the purpose of comparison, the harmonic spectra for atomic systems with $I_p = 32.54$ a.u. (corresponding to Kr^{20+}) and $\omega = 1$ a.u., and with $I_p = 4.42$ a.u. (corresponding to Ne^{4+}) and $\omega = 0.05$ a.u. are computed. The appropriate field and atomic parameters for these potentials, shown in Table I, are chosen to make sure that the ionization by the strong laser field is in the tunneling regime with the Keldysh parameter $\gamma = \sqrt{I_p/(2U_p)} < 1$, with comparable ionization probabilities for all cases (the ionization probability is 0.9 in the case of $I_p = 32.54$ a.u., $\omega = 1$ a.u., and 0.4 in the case $I_p = 4.42$ a.u., $\omega = 0.05$ a.u.), and that the HHG plateau (cutoff) energy is of order of the ionization potential

TABLE I. Ionization energies and laser parameters used for calculations.

I_p (a.u.)	q	ω (a.u.)	I_0 (W/cm^2)	ξ	γ	$\omega_{\rm max}$ (a.u.)	α_0 (a.u.)
112.2	52	3	2×10^{20}	0.1836	0.595	651	8.39
112.2	52	1	2×10^{20}	0.5509	0.198	4669	75.49
32.54	21	1	8.5×10^{18}	0.1136	0.518	235.2	15.56
4.42	5	0.05	3×10^{16}	0.1349	0.161	277.1	369.83

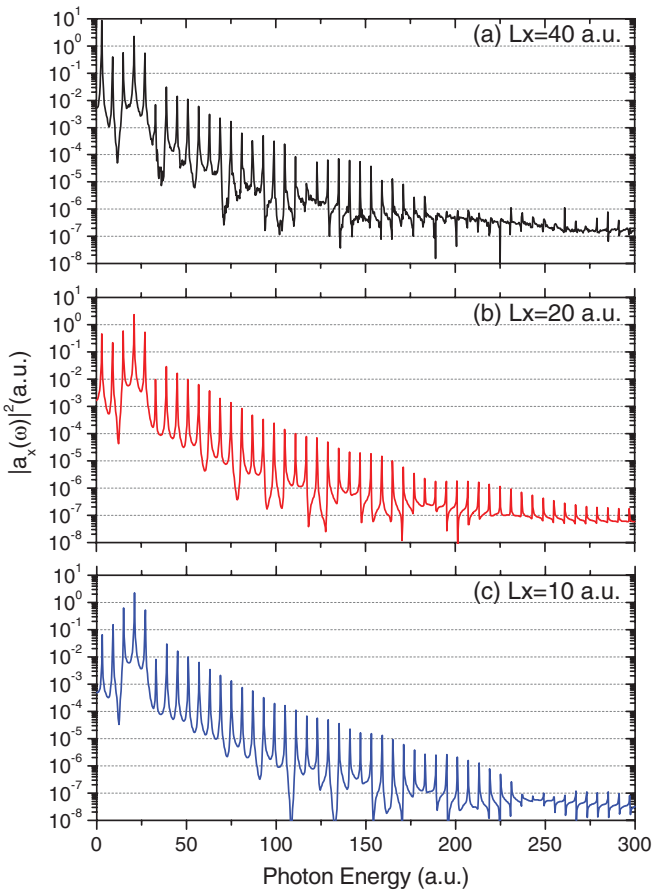

FIG. 2. (Color online) The below-threshold harmonic spectra in the case of $I_p = 112.2$ a.u., $\omega = 3$ a.u., and laser intensity $I_0 = 2 \times 10^{20}$ W/cm^2, obtained for different box sizes applied in the simulation.

for the BTH generation. Figure 1 clearly indicates that, for a fixed emitted harmonic photon energy, e.g., $\omega_H = 110$ a.u., the absolute yield of the BTH for a tightly bound system (Pb^{51+}, $I_p = 112.2$ a.u.) induced by the high-energy photons ($\omega = 3$ a.u.) is larger by more than three orders of magnitude than the three-step HHG from HCIs of a smaller charge (Kr^{20+}, $I_p = 32.54$ a.u. and $\omega = 1$ a.u.) and by more than 12 orders magnitude than the three-step HHG driven by an infrared laser field (Ne^{4+}, $I_p = 4.42$ a.u. and $\omega = 0.05$ a.u.). One can infer from Fig. 2 that the reason for this is the different nature of the BTH process: For BTH essentially bound dynamics is responsible for emission. However, tunneling harmonics occur only with a weaker potential where the recolliding wave packets undergo large continuum excursion (see Table I), suffering from spreading, which leads to a small single-atom efficiency of the process.

It is worth noting that Hu *et al.* [16–18] studied the nontunneling high-order harmonics from ultraintense-laser-driven tightly bound systems. The low-order-harmonic spectra they obtained showed the existence of a spectral plateau with a well-defined cutoff, which was explained by a "surfing" mechanism of the electron in the effective potential. However, this kind of plateau is absent in our calculations, which is probably connected with the fact that the surfing regime of

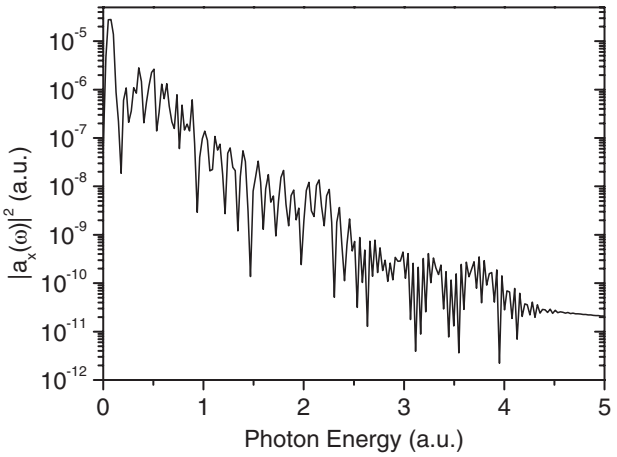

FIG. 3. The HHG spectrum for a neon atom in a linearly polarized laser pulse of sub-1.5-cycle duration with a wavelength $\lambda = 720$ nm and an intensity of $I_0 = 5.8 \times 10^{14}$ W/cm^2. The parameters correspond to the experiment of [49].

HHG is very sensitive to the laser and atomic parameters and is not realized in the considered case.

To have an idea on the absolute yield of BTH, we show in Fig. 3 a typical example for low-energy HHG at $\omega_H \sim 80$ eV realized in the experiment of Goulielmakis *et al.* [49]. In this experiment sub-100-as pulses containing ~0.5 nJ of energy with the single-photon energy of ~80 eV were measured with a conversion efficiency of $\sim 10^{-6}$. In Fig. 3, we have calculated the single-atom HHG response for the above-mentioned experimental parameters: neon atoms in a linearly polarized 720 nm laser field with $I_0 = 5.8 \times 10^{14}$ W/cm^2. The spectrum is obtained by numerical simulation of the 3D nonrelativistic TDSE with the code QPROP [50]. We see that the yield of BTH for a single-atom response in Fig. 1 is orders of magnitude higher than that of the single neon atom shown in Fig. 3. This indicates the real chances for BTH generation.

Additionally, we estimate the total photon number per shot emitted from a typical gas target in the BTH regime for the black highest curve in Fig. 1. From the acceleration we can deduce the spectral density of the emitted photon number per solid angle of a single atom as [51]

$$\frac{d^2N}{d\Omega\, d\omega_H} = \frac{\sin^2\theta}{4\pi^2 c^3 \omega_H} |a_x(\omega_H)(T_2 - T_1)|^2, \tag{8}$$

where Ω is the solid emission angle. Under perfect phase-matching conditions the total emitted photon number is given as

$$N = (\rho V)^2 \int d\omega_H \frac{d^2N}{d\Omega\, d\omega_H} \Delta\Omega(\omega_H), \tag{9}$$

where ρ is the number density of the gas and V the contributing volume. The solid emission angle is approximated by $\Delta\Omega(\omega_H) \sim \pi\theta^2$, with the angular width $\theta \sim 2\pi c/D\omega_H$ of the central speckle of an interference pattern caused by a circular aperture of diameter D. As the length of the medium we choose the coherence length $l_{\rm coh} = \pi c/[\omega_H(1 - n_e)]$ in a free-electron gas, where $n_e = \sqrt{1 - \omega_p^2/\omega^2}$ is the refractive index, with the plasma frequency $\omega_p = \sqrt{4\pi Z\rho}$ and the

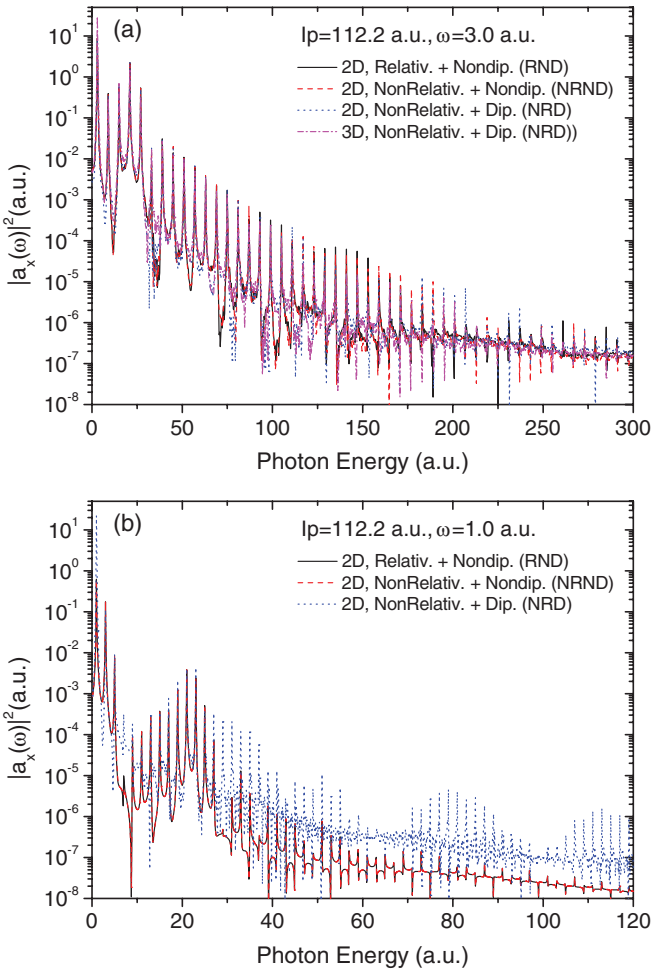

FIG. 4. (Color online) The relativistic and nondipole effects on the photon emission of an electron in the soft-core potential of $I_p = 112.2$ a.u. exposed to a laser field with an intensity of 2×10^{20} W/cm^2 and photon energy of $\omega = 3$ a.u. (a) and $\omega = 1$ a.u. (b). The other parameters are the same as in Fig. 1 and are shown in Table I.

number of free electrons per atom Z. For a gas density of $\rho = 10^{17}/\text{cm}^3$ and an ion charge $Z = 51$, we find a coherence length on the order of 1 mm in the center of the harmonic spectrum. Assuming a gas target of diameter $D = 10\,\mu$m, we calculate an emitted photon number of 10^7 for the spectral window between 6 and 100 a.u. from Eq. (9). The number is competitive with results of standard nonrelativistic experiments despite the low gas density and tiny emission angle at these high energies. The pulse energy of the applied driving XUV pulse is 200 μJ in the considered case, yielding a conversion efficiency of 10^{-8}.

To find the impact of the magnetic components of the laser field and the relativistic mass shift on the photon emission process for BTH, the HHG spectra obtained with the dipole approximation and with the nondipole nonrelativistic approximation by omitting the relativistic mass shift term in the Hamiltonian of Eq. (1) are shown in Fig. 4. The nonrelativistic TDSE calculations in dipole approximation using the 3D QPROP code with a Crank-Nicolson propagator is also shown for comparison. Figure 4(a) shows the harmonic spectra for $I_p = 112.2$ a.u. and $\omega = 3$ a.u. For those parameters

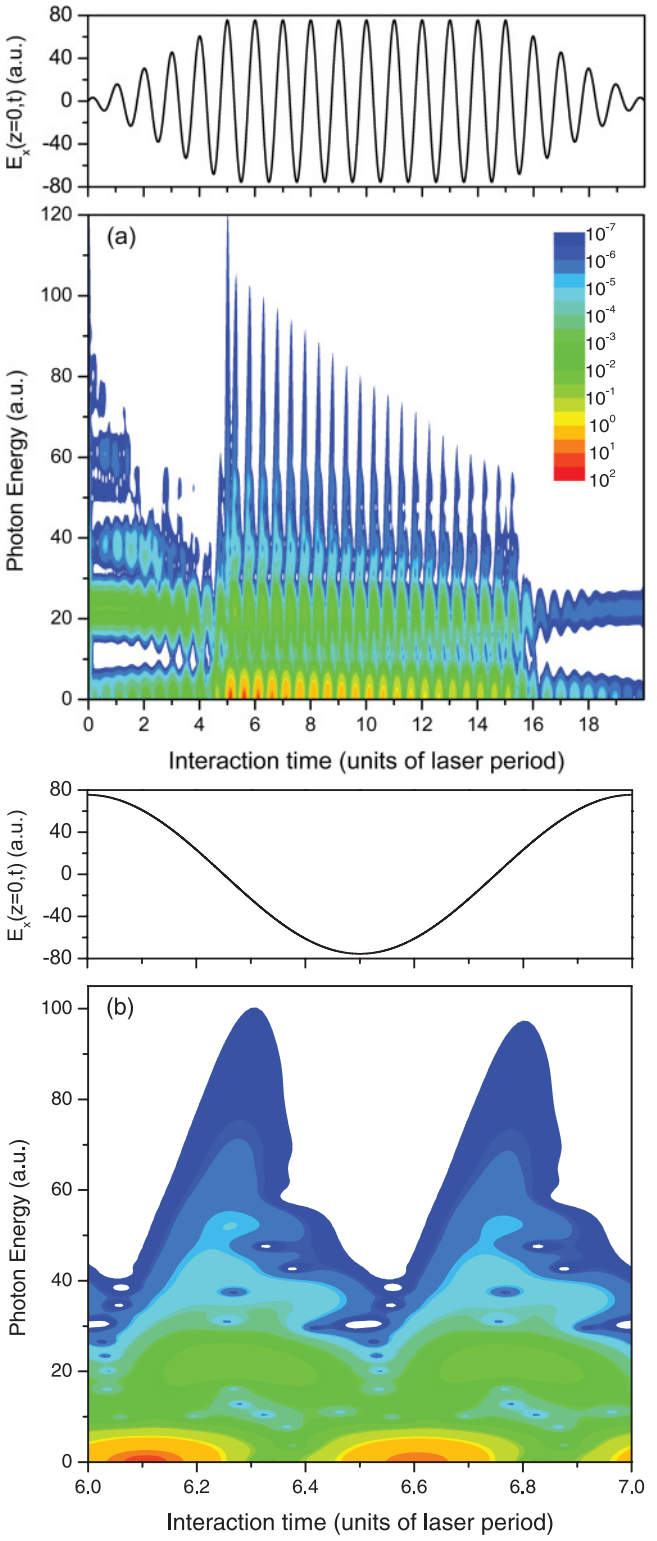

FIG. 5. (Color online) Time-frequency analysis of the electron acceleration (3) by use of Eq. (5) with a time window of $\Delta t = 0.05T$. The other parameters are the same as in Fig. 1 with $I_p = 112.2$ a.u. and $\omega = 1$ a.u.. In (a) we show the total analysis whereas in (b) the seventh cycle is shown in more detail. The upper panels in (a) and (b) show the time dependence of the laser field.

the relativistic corrections are negligible. The 2D and 3D results show a similar spectral distribution, which

indicates that for this tightly bound system the electron wave packet spreading plays no essential role in the BTH generation and converges within a discrepancy smaller than one order of magnitude. In the case of $I_p = 112.2$ a.u. and $\omega = 1$ a.u. [see Fig. 4(b)], the magnetically induced drift in the laser propagation direction shows a strong influence on HHG spectra for higher photon energies ω_H, in contrast to the $\omega = 3$ a.u. case. Harmonics larger than $\omega_H \gtrsim 40$ a.u. are damped by more than one order of magnitude, which is because of a rather large $\xi \approx 0.55$. The role of the relativistic drift is quantified by the parameter $\eta \equiv \sqrt{2I_p}\xi^3 c/\omega$ which is defined in [36] as the ratio of the drift distance in the laser propagation direction to the electron wave packet spreading during a laser period. $\eta = 0.27$ in the case of $I_p = 112.2$ a.u., $\omega = 3$ a.u. and $\eta = 21$ at $I_p = 112.2$ a.u., $\omega = 1$ a.u. ($\eta = 2.1$ in the case of $I_p = 4.42$ a.u., $\omega = 0.05$ a.u.), giving an explanation for the conspicuous damping impact of the relativistic drift in the $\omega = 1$ a.u. case. An unexpected fact is that the relativistic drift can have an impact not only in the three-step regime of HHG but also in the BTH regime where the bound dynamics dominates, damping the high-energy tail of BTHs. This could be the reason why we do not observe the same enhancement for the BTH with $I_p = 112.2$ a.u. and $\omega = 1$ a.u. (dashed red line in Fig. 1) as the for the case of $\omega = 3$ a.u. (top black solid line). In fact the BTHs for $I_p = 112.2$ a.u. and $\omega = 1$ a.u. (dashed red line) have a lower yield comparable to that of the tunneling harmonics (dotted blue line). Figure 4(b) indicates also that the relativistic mass shift still does not play a role in the BTH regime at this ξ value. For $\omega = 1$ a.u. [Fig. 4(b)] we were not able to obtain convergent 3D numerical results within a practical time span. Although both the split-operator and the Crank-Nicolson propagators are claimed to be accurate to the second order in the time step, we found that a much smaller time step is required for the convergence of the QPROP calculations. We employed $dt = 3.2 \times 10^{-4}$ a.u. for the convergent results of Fig. 4(a). For $\omega = 1$ a.u. we decreased the time step down to $dt = 1.2 \times 10^{-4}$ a.u., which was not sufficient to obtain convergence for the high-energy tail of the spectrum. For this reason we do not show the results in Fig. 4(b). Nevertheless, in the low-energy part of the spectrum convergence occurred and we found agreement between these 3D results and the nonrelativistic 2D results within the dipole approximation (dashed blue line), as in Fig. 4(a). The bottom line is that the observations justify the restriction to a two-dimensional grid for the problem under investigation.

To gain more insight into the BTH generation, we have carried out a time-frequency analysis using a window Fourier transformation based on Eq. (5); see Fig. 5. In Fig. 5(a), we distinguish two signatures: On the one hand, the horizontal emission areas below 10 a.u. and at about 20, 40, 60, and 80 a.u. with an enhanced HHG yield are recognizable on the time-frequency map. The corresponding energies of the areas depend only on the atomic potential and the driving laser field intensity but not on the driving laser frequency. They match the transition energies of the bound system. Therefore, we think those photon energies correspond to a bound-bound transition between Stark-shifted states. On the other hand, spikelike structures within the plateau of the driving pulse between 5 and 15 optical cycles are visible, which are responsible for the high-frequency BTHs. Both signatures lose strength in the course of time because they are affected by depletion due to ionization.

As an example, we discuss the seventh cycle in Fig. 5(b). We observe a periodic resonant emission at the photon energies $\omega_H < 10$ a.u. and $\omega_H \approx 20$ a.u. Two characteristic regions of BTHs can be identified in Fig. 5(b) based on the characteristic time of the harmonic emission, i.e., low-frequency BTHs with $\omega_H < 10$ a.u. and high-frequency BTHs with 10 a.u. $< \omega_H < I_p$. The low-frequency BTHs are emitted near the peak of the laser field with a slight phase delay. The emission times of the high-frequency BTHs 20 a.u. $< \omega_H < I_p$ form a bowlike structure which recalls the one well known from tunneling HHG; cf. Fig. 3 in [11]. In contrast to the usual three-step HHG, here the widths of the bowlines for the emission time are rather broad, which indicates that the quasiclassical description is less applicable for BTHs than for the above-threshold harmonics. The emission times of the low-frequency BTHs relative to the high-frequency BTHs indicate that they are probably due to the L-type quantum orbit [11] of the essentially bound electron.

Figure 5(a) shows that the depletion of the bound state has the largest impact on the long trajectories (see the right part of the bowlike structure), i.e., the long trajectories of BTHs are more vulnerable to the influence of the Coulomb field of the atomic core. These findings require further investigation.

V. SUMMARY

The interaction of a tightly bound single-active-electron system with an ultraintense laser field in the weakly relativistic regime is investigated by numerical solution of the two-dimensional weakly relativistic Schrödinger equation in which the nondipole effects and the relativistic mass shift correction are included. The strong-field approximation is not accurate enough to describe the dynamics of the electronic wave packet in the XUV field because of the increased importance of the atomic potential. Within the intensities considered, the relativistic mass shift effect is found to be much smaller than the nondipole effect. The plateau and the well-defined cutoff which characterized the standard tunneling-recombination HHG are absent in the below-threshold harmonic spectrum which we have obtained. However, the intensity of these harmonics is found to be orders of magnitude stronger than that of the standard above-threshold harmonics of the same photon energy. By use of highly charged ions with a large atomic number, it is expected that highly efficient below-threshold harmonics can be extended to the higher-energy region, which opens a way for the generation of coherent hard-x-ray radiation from the harmonic emission processes. On the other hand, we should also recall that the radiation signal generated in a strong-field laser-matter interaction is determined not only by the radiation pattern from a single ion, but also by the phase-matching process during propagation. We provided a preliminary estimate for the macroscopic yield showing that 10^7 harmonic photons in the keV energy range can be obtained in the BTH regime with an efficiency of 10^{-8}. However, accurate investigations of the macroscopic propagation effects based on a solution of the Maxwell equations are required

in order to draw a reliable conclusion about the applicability of below-threshold harmonics for coherent hard-x-ray generation.

ACKNOWLEDGMENT

We would like to thank Heiko Bauke for supporting the numerical calculations.

[1] M. Ferray, A. L'Huillier, X. F. Li, L. A. Lompre, G. Mainfray, and C. Manus, J. Phys. B **21**, L31 (1988).
[2] P. Agostini and L. F. DiMauro, Rep. Prog. Phys. **67**, 813 (2004).
[3] F. Krausz and M. Ivanov, Rev. Mod. Phys. **81**, 163 (2009).
[4] P. B. Corkum, Phys. Rev. Lett. **71**, 1994 (1993).
[5] K. J. Schafer, B. Yang, L. F. DiMauro, and K. C. Kulander, Phys. Rev. Lett. **70**, 1599 (1993).
[6] M. Lewenstein, P. Balcou, M. Yu. Ivanov, A. L'Huillier, and P. B. Corkum, Phys. Rev. A **49**, 2117 (1994).
[7] W. Becker, S. Long, and J. K. McIver, Phys. Rev. A **50**, 1540 (1994).
[8] M. B. Gaarde, F. Salin, E. Constant, Ph. Balcou, K. J. Schafer, K. C. Kulander, and A. L'Huillier, Phys. Rev. A **59**, 1367 (1999).
[9] P. Salières *et al.*, Science **292**, 902 (2001).
[10] L. V. Keldysh, Zh. Eksp. Teor. Fiz. **47**, 1945 (1964) [Sov. Phys. JETP **20**, 1307 (1965)]; F. H. M. Faisal, J. Phys. B **6**, L89 (1973); H. R. Reiss, Phys. Rev. A **22**, 1786 (1980).
[11] D. B. Milošević and W. Becker, Phys. Rev. A **66**, 063417 (2002).
[12] D. C. Yost *et al.*, Nat. Phys. **5**, 815 (2009).
[13] E. P. Power *et al.*, Nat. Photon. **4**, 352 (2010).
[14] J. A. Hostetter, J. L. Tate, K. J. Schafer, and M. B. Gaarde, Phys. Rev. A **82**, 023401 (2010).
[15] H. Soifer *et al.*, Phys. Rev. Lett. **105**, 143904 (2010).
[16] S. X. Hu, D. B. Milošević, W. Becker, and W. Sandner, Phys. Rev. A **64**, 013410 (2001).
[17] S. X. Hu, A. F. Starace, W. Becker, W. Sandner, and D. B. Milošević, J. Phys. B **35**, 627 (2002).
[18] S. X. Hu and C. H. Keitel, Phys. Rev. A **63**, 053402 (2001).
[19] [https://slacportal.slac.stanford.edu/sites/lcls_public/Pages/Default.aspx], [http://www.xfel.eu/].
[20] J. Seres *et al.*, Nature (London) **433**, 596 (2005).
[21] E. Goulielmakis *et al.*, Science **320**, 1614 (2008).
[22] T. Popmintchev *et al.*, Proc. Natl. Acad. Sci. USA **106**, 10516 (2009).
[23] M.-C. Chen, P. Arpin, T. Popmintchev, M. Gerrity, B. Zhang, M. Seaberg, D. Popmintchev, M. M. Murnane, and H. C. Kapteyn, Phys. Rev. Lett. **105**, 173901 (2010).
[24] T. Popmintchev, M.-C. Chen, P. Arpin, M. M. Murnane, and H. C. Kapteyn, Nat. Photon. **4**, 822 (2010).
[25] Y. I. Salamin, S. X. Hu, K. Z. Hatsagortsyan, and C. H. Keitel, Phys. Rep. **427**, 41 (2006).
[26] N. J. Kylstra *et al.*, Phys. Rev. Lett. **85**, 1835 (2000).
[27] C. C. Chirilă, N. J. Kylstra, R. M. Potvliege, and C. J. Joachain, Phys. Rev. A **66**, 063411 (2002).
[28] G. Mocken and C. H. Keitel, J. Phys. B **37**, L275 (2004).
[29] C. C. Chirilă, C. J. Joachain, N. J. Kylstra, and R. M. Potvliege, Phys. Rev. Lett. **93**, 243603 (2004).
[30] B. Henrich, K. Z. Hatsagortsyan, and C. H. Keitel, Phys. Rev. Lett. **93**, 013601 (2004).
[31] N. Milosevic, P. B. Corkum, and T. Brabec, Phys. Rev. Lett. **92**, 013002 (2004).
[32] Q. Lin, S. Li, and W. Becker, Opt. Lett. **31**, 2163 (2006).
[33] M. Verschl and C. H. Keitel, Phys. Rev. Spec. Top. Accel. Beams **10**, 024001 (2007).
[34] M. Klaiber, K. Z. Hatsagortsyan, and C. H. Keitel, Phys. Rev. A **75**, 063413 (2007).
[35] M. Klaiber, C. Müller, K. Z. Hatsagortsyan, and C. H. Keitel, Opt. Lett. **33**, 411 (2008).
[36] K. Z. Hatsagortsyan, M. Klaiber, C. Müller, M. C. Kohler, and C. H. Keitel, J. Opt. Soc. Am. B **25**, 93 (2008).
[37] M. C. Kohler, M. Klaiber, K. Z. Hatsagortsyan, and C. H. Keitel, Europhys. Lett. **94**, 14002 (2011).
[38] Alternatively, HCIs with high purity and high density can be generated by sending atoms through thin foils [see, e.g., J. R. Crespo López-Urrutia *et al.*, J. Phys.: Conf. Ser. **2**, 42 (2004)]; or from interaction of intense laser fields with atomic, ionic, or multicenter molecular cluster targets [see, e.g., E. M. Snyder, S. A. Buzza, and A. W. Castleman Jr., Phys. Rev. Lett. **77**, 3347 (1996); T. Ditmire *et al.*, *ibid.* **78**, 2732 (1997)].
[39] S. Augst, D. Strickland, D. D. Meyerhofer, S. L. Chin, and J. H. Eberly, Phys. Rev. Lett. **63**, 2212 (1989).
[40] W. Ackermann *et al.*, Nat. Photon. **1**, 336 (2007); [http://flash.desy.de/photon_science/].
[41] K. C. Kulander, K. J. Schafer, and J. L. Krause, Int. J. Quantum Chem. **25**, 415 (1991).
[42] M. Klaiber, K. Z. Hatsagortsyan, and C. H. Keitel, Phys. Rev. A **71**, 033408 (2005).
[43] S. Palaniyappan, I. Ghebregziabher, A. DiChiara, J. MacDonald, and B. C. Walker, Phys. Rev. A **74**, 033403 (2006).
[44] G. R. Mocken and C. H. Keitel, Comput. Phys. Commun. **166**, 171 (2005).
[45] K. Burnett, V. C. Reed, J. Cooper, and P. L. Knight, Phys. Rev. A **45**, 3347 (1992).
[46] M. D. Feit, J. A. Fleck, and A. Steiger, J. Comput. Phys. **47**, 412 (1982).
[47] J. A. Fleck, J. R. Morris Jr., and M. D. Feit, Appl. Phys. **10**, 129 (1976).
[48] J. L. Krause, K. J. Schafer, and K. C. Kulander, Phys. Rev. A **45**, 4998 (1992).
[49] E. Goulielmakis *et al.*, Science **320**, 1614 (2008).
[50] D. Bauer and P. Koval, Comput. Phys. Commun. **174**, 396 (2006).
[51] L. D. Landau and E. M. Lifshitz, *The Classical Theory of Field* (Pergamon, London, 1975).